Am J Clin Exp Urol 2025;13(3):194-214
www.ajceu.us /ISSN:2330-1910/AJCEU0163907

Original Article

Comparative transcriptome profiling of the lumbosacral dorsal root ganglia reveals sexually dimorphic gene expression in a murine model of coronavirus-induced neurodegeneration

Taylor C Foley*, Sathish K Yesupatham*, Jake Miller-Dawson, Anna P Malykhina

Division of Urology, Department of Surgery, University of Colorado Anschutz Medical Campus, Aurora, CO, USA.
**Equal contributors.*

Received February 13, 2025; Accepted May 26, 2025; Epub June 15, 2025; Published June 30, 2025

Abstract: Introduction: Neuroinflammation of the central nervous system (CNS) triggers long-lasting neurodegenerative changes associated with the development of neurogenic dysfunction in the pelvic organs. We previously described the symptoms of voiding dysfunction in a mouse model of multiple sclerosis (MS) induced by a coronaviral infection with mouse hepatitis virus (MHV). The aim of the current study was to identify immune, inflammatory and neuronal changes in the lumbosacral (L6-S2) dorsal root ganglia (DRG) innervating the lower urinary tract (LUT) after severe neurodegeneration in the CNS. Methods: Adult C57BL/6 male (N=18) and female (N=18) mice received either an intracranial injection of MHV (coronavirus-induced encephalomyelitis, CIE group), or sterile saline (control group). Dorsal root ganglia were collected from mice of both sexes at 1 and 4 weeks, followed by isolation of total RNA and bulk RNA sequencing. Results: Transcriptome analysis of LS DRG identified a sex dependent expression of the genes at baseline with females having an increased expression of the immune system and extracellular matrix (ECM) related differentially expressed genes (DEGs) whereas males showed an upregulation of the genes belonging to protein synthesis, folding, and post-translational phosphorylation. Acute neuroinflammation (1 wk post-infection) triggered extensive immune responses involving the families of interferons (*Ifna2, Ifng, Ifnl1*), interleukins (*Il1a, Il1b, Il6*), toll-like receptors (*Tlr9, Tlr7*), and guanylate-binding proteins (GTPases, *Gbp*) in both, CIE males and females. However, at a later stage of neurodegeneration (4 wks post-infection), the number of upregulated DEGs was down 6-fold in CIE males, whereas in CIE females the downregulated pathways were predominant, and mostly included genes encoding motor proteins (*Myh7*, *Myl2, Myl3, Tnnt1, Tnnl1, Dnah5*). Among the pathways upregulated in males but downregulated in females at both time points were phagosome formation pathway, neutrophil extracellular trap signaling, and hepatic fibrosis pathway. Conclusions: This study confirmed a differential expression of immune, inflammatory, and neural DEGs in sensory ganglia of male and female mice undergoing CNS neurodegeneration and neuroinflammation. The obtained results suggest a functional role of sex-dependent sensory interoception in the development of neurogenic LUTS in a coronavirus-induced murine model of MS.

Keywords: Sensory ganglia, lower urinary tract, bulk RNAseq, neurodegeneration, neurogenic LUTS

Introduction

Lower urinary tract symptoms (LUTS) develop in patients with neurodegenerative diseases affecting the central nervous system (CNS). Multiple sclerosis (MS) is one of these conditions of unknown etiology characterized by demyelinated lesions in the CNS, and a variety of symptoms from fatigue and difficulties with coordination to the loss of bowel, urinary, and sexual function [1, 2]. Neurogenic LUTS develop in a majority of MS patients, and the frequency and type of bladder symptoms substantially rise with disease progression and development of physical disability [3, 4]. The most common LUTS include urgency, increased frequency of micturition, incontinence, detrusor overactivity, hesitancy, weak urine stream, urinary retention, nocturia, and dysuria [3, 5]. Most of these symptoms start from the altered sensation in the lower urinary tract (LUT) regulated by the activity of primary afferent neurons innervating

https://doi.org/10.62347/SLKE7419

the urinary bladder. Afferent innervation of the LUT originates from the thoracolumbar and lumbosacral (LS) dorsal root ganglia (DRG) where the cell bodies of bladder sensory neurons reside [6].

Dorsal root ganglion neurons are the first order extrinsic neurons receiving afferent information from the urinary bladder (UB) with specialized anatomical and functional properties. A unique morphological feature of DRG neurons is their pseudo-unipolarity with a single T-type axon leaving the soma and splitting into the central and peripheral axonal branches close to the neuronal cell body [7]. The unique anatomy of sensory neurons comes in combination with their dual "afferent-efferent" function. They express a variety of sensory receptors and ion channels that can detect physical, chemical, thermal, and environmental stimuli followed by the transmission of information to the CNS where the sensory signals are integrated, processed, and coordinated [8]. In addition to afferent function, distal axonal branches of DRG neurons can release sensory neuromodulators (*i.e.* calcitonin gene-related peptide and substance P) in the periphery, thereby, producing "efferent function" in the innervated organs by promoting local neurogenic inflammation [9], cell proliferation, or tissue regeneration [10].

Recent bulk and single cell RNAseq studies of DRG confirmed sex-dependent expression profiles in mice [11-13] and human [14, 15] specimens from physiological and diseased conditions, including MS [16, 17]. Women are twice as likely to develop MS as men, whereas disease progression and disability seem to advance more rapidly in men [18]. Sex differences related to UB function and voiding symptoms have been reported in MS patients as well [19]. A recent longitudinal study of LUTS in MS patients determined a higher percentage of under-recorded, moderate to severe LUTS in females in comparison to males that were not correlated with reproductive factors such as menopausal status or parity [20]. Additionally, by year 10 of disease duration, female sex and relapsing MS subtype were predictive of worsening LUTS in comparison to males [20].

Animal models also provided a growing body of evidence that innate and adaptive immune responses may be different in males and females [21-24]. Our group previously described neurogenic LUTS in a murine model of coronavirus-induced encephalomyelitis (CIE) [25-27], a validated animal model of MS with Spontaneous onset of neuroinflammation in the CNS and a robust innate immune response that mimics the pathophysiology of human MS [28-30]. We established that neurogenic LUTS developed in parallel with activation of gliosis in the CNS, increased expression of pro-inflammatory cytokines, altered nerve-mediated contractions of the detrusor, accumulation of inflammatory mediators in the UB, and distinct transcriptomic and proteomic profiles of macrophages and cytotoxic cells [31-33]. However, we did not test whether the occurrence of LUTS could be associated with altered physiological properties of UB sensory innervation. Therefore, in the current study, we used a general transcriptomic approach (bulk RNAseq) to characterize the molecular profiles of LS DRG neurons collected from adult male and female CIE mice. Computational analysis uncovered differentially expressed genes (DEGs) in sensory ganglia of both sexes at the baseline and after a coronaviral infection. The obtained datasets provide a valuable resource of molecular and secretory targets that can be leveraged for understanding sex differences in sensory modulation of neurogenic LUTS associated with MS pathology.

Methods

Animals and experimental groups

The study used 36 adult C57BL/6J mice (18 females and 18 males, 12 wks of age) purchased from Jackson Laboratory (Bar Harbor, ME). Mice were housed in a temperature-regulated animal facility in the University of Colorado, Anschutz Medical Campus (CU-AMC) vivarium on a 14-hour light/10-hour dark cycle. All mice had *ad libitum* access to food and water with special measures taken to accommodate neurologically compromised animals. Animal procedures were performed according to the protocols approved by the University of Colorado Institutional Animal Care and Use Committee in accordance with relevant guidelines and regulations (IACUC protocol #00472). The reporting of experimental animal data in the manuscript follows the recommendations in the ARRIVE guidelines (https://arriveguidelines.org/arrive-guidelines).

Mouse model of coronavirus-induced encephalomyelitis (CIE)

Mice received either a single intracranial injection of 20 µl sterile saline (N=12, control group) or mouse hepatitis virus (MHV, A59 strain, 6000 PFU, N=24, CIE groups) in 20 µl sterile saline under isoflurane anesthesia, as previously described [31, 34]. After viral injection, mice were weighed and monitored daily for assessment of neurological symptom development by using clinical symptom score (CSS). Clinical symptom score was used to assess and compare the degree of neurodegenerative symptoms based on the following scale: 0=normal with no clinical signs, 1=loss of tail tonicity/kyphosis, 2=tail paralysis/severe kyphosis, 3=partial hindlimb paralysis, 4=complete hindlimb paralysis, and 5=complete hindlimb paralysis and forelimb paresis/paralysis, as previously described [31, 33]. We also evaluated additional neurological parameters with "yes" or "no" answers including the lack of grooming, eye and/or nose discharge, lethargic behavior, tail paresis and orbital tightening. Due to the risk of viral transmission to other mice, control and CIE mice were housed in separate cages on separate racks within the ABSL2 facility. Mice showing weight loss or signs of distress were supplemented with food and HydroGel packets (ClearH_2O, Westbrook, ME) on the bottom of the cage. For euthanasia procedure, mice were deeply anesthetized with isoflurane followed by cervical dislocation in accordance with recommendations of the Panel on Euthanasia of the American Veterinary Medical Association [35].

Voiding spot assay

The spontaneous voiding spot assay (VSA) was used to evaluate the severity of LUTS in CIE and saline-injected mice at the baseline, and then weekly until experimental end points. Single mice were transferred into individual cages with absorbent filter paper on the bottom of the cage with *ad libitum* access to water but no food for 3 hours (10 am to 1 pm). No acclimation was performed prior to testing. Animals were returned to their housing cages after the assay. Ultraviolet light was used to image voiding spots on the filter paper. We used Image J (Bethesda, MD) to record the total voided area, and the number of large (≥0.5 cm^2) and small (≤0.5 cm^2) voided spots for each filter paper.

Isolation of DRG and RNAseq protocol

Lumbosacral DRG were collected from the control groups (N=3 per sex per time point, total N=12), during the acute stage of infection (N=6 per sex at 1 wk, total N=12), and at the first peak of demyelination (N=6 per sex at 4 wks, total N=12). Isolated DRG were immediately placed on dry ice for freezing, and then stored at -80°C. Total RNA was extracted using RNAeasy miniprep kit (Qiagen, CA, USA) following the manufacturer's instructions. Isolated RNA was re-suspended in RNase-free water and stored at -80°C. RNA quantification was done using Qubit fluorometer 3.0 (ThermoFisher Scientific, USA), and 200 ng of RNA per sample was used for library preparation. RNA Quality check was performed on Agilent 2100 bioanalyzer (ThermoFisher Scientific, USA). Library preparation was carried out by the CU-AMC Genomics Core facility using universal mRNA Poly-A tail prep kit. The libraries which passed the quality check were sequenced at a depth of 40 million paired-end reads per sample on a Novaseq platform (Illumina, USA).

Statistical analyses

Statistical analyses of body weight, CSS and VSA datasets were done using GraphPad Prism 10 (GraphPad Software, La Jolla, CA). Two-way ANOVA was performed to compare data among tested time points, treatments and between sexes. Data found statistically significant by ANOVA were analyzed using two-tailed unpaired t-test between two groups. A p value ≤0.05 was considered statistically significant. Unless stated otherwise, the results are expressed as mean ± standard error of the mean (SEM). Figures were prepared using GraphPad Prism 10 (GraphPad Software, La Jolla, CA) and Microsoft PowerPoint (Microsoft Office Suite Software, Redmont, WA).

Analysis of bulk RNAseq data was conducted using Partek® Flow® (Version 10.0; Partek Inc., USA). The raw FASTQ files were uploaded, and quality check for the reads was performed. Reads were aligned to mouse reference genome (mm10) using STAR aligner (STAR - 2.7.8a). HTSeq (0.11.0) was used for annotation and quantification. Gene expression analysis was performed using DESeq2. Datasets were analyzed by using sex (male *vs* female) and treatment (saline *vs* MHV) as determi-

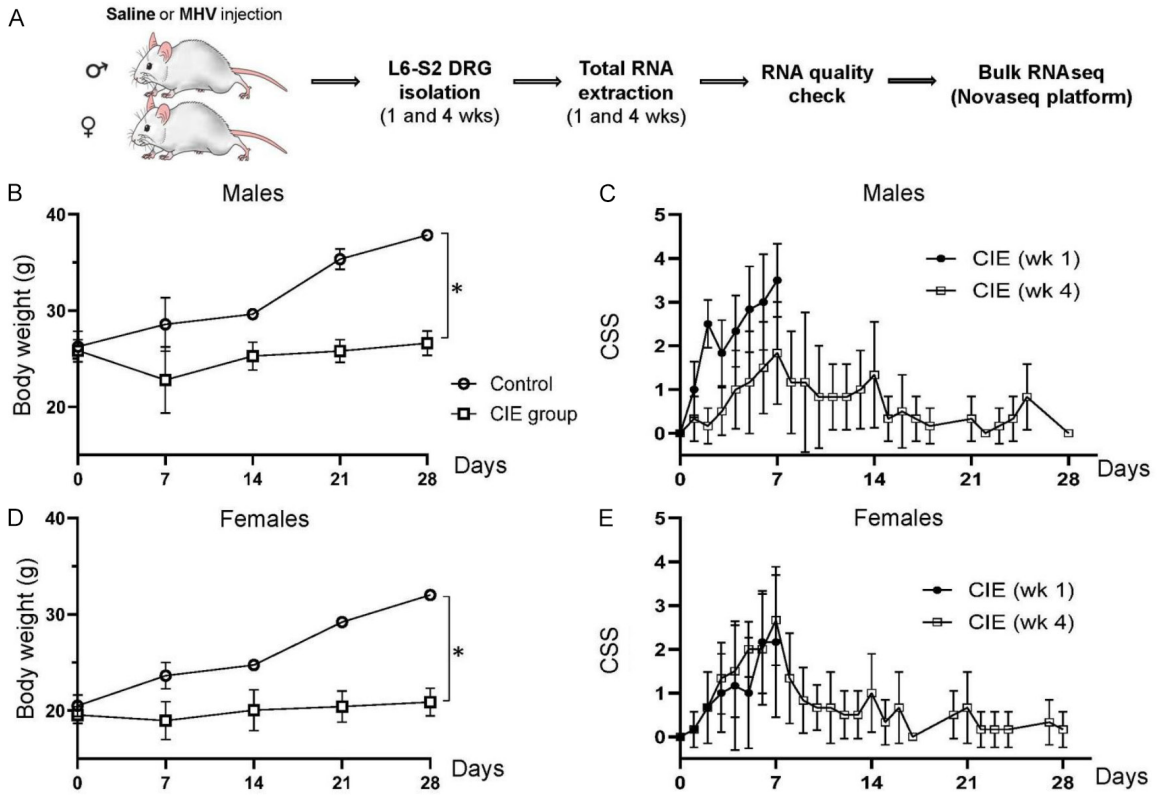

Figure 1. Schematic presentation of the study design and assessment of neurological clinical symptoms in CIE mice. A. Experimental design of the study and RNAseq approach. B. Changes in the body weight in control and CIE male mice up to 4 wks post-infection (*P<0.001 to control group). C. Clinical symptom score (CSS) development during CIE progression in male mice. D. Body weight in control and CIE females during disease progression (*P<0.001 to control group). E. Average daily CSS values for CIE female mice. *P<0.05 to respective control groups.

nants. Gene expression data were downloaded as Excel files and used to perform Ingenuity Pathway Analysis (IPA) using IPA software (Qiagen, USA). The cut-off values for genes to be included in pathway analyses were +/-1.5-fold change with *p*-value ≤0.05. IPA software was used to create volcano plots, pathway tables, and Venn diagrams. Data on functional pathway activation changes from IPA software was used to create pie charts in Excel by dividing the number of the genes within a pathway from our dataset by the overall number of differentially expressed genes (DEGs).

Results

Sex differences in neurological clinical symptoms and voiding function in CIE mice

To evaluate the effects of coronavirus-induced neuroinflammation on neurological symptoms and micturition patterns of mice, we recorded animal weights, CSS and micturition patterns daily in all animals up to 4 wks post-infection. The workflow of experimental study design is included in **Figure 1A**. Male CIE mice experienced 12% weight loss at 1 wk post-MHV infection, followed by a slow recovery to the baseline weight of 25.8±0.5 g at 3 and 4 wks (**Figure 1B**). Control group of age-matched males steadily gained weight from 26.3±0.6 g at the baseline to 37.8±0.2 g (43.7% increase, P≤ 0.001) at 4 wks post-infection (**Figure 1B**). The absence of weight gain in CIE males correlated with a significant increase in CSS, reaching 3.5±0.3 score in the 1 wk group at 7 days post-infection in comparison to a CSS of 1.8±0.5 in the 4 wks group (P≤0.05 to day 0 for each group, **Figure 1C**), consistent with previously published by our group data [31, 33]. Similar changes in the body weight and CSS values were recorded in the female groups. Female mice stopped gaining weight immediately after inoculation with the virus, and body weight increased by only 6.7% at 4 wks post-infection

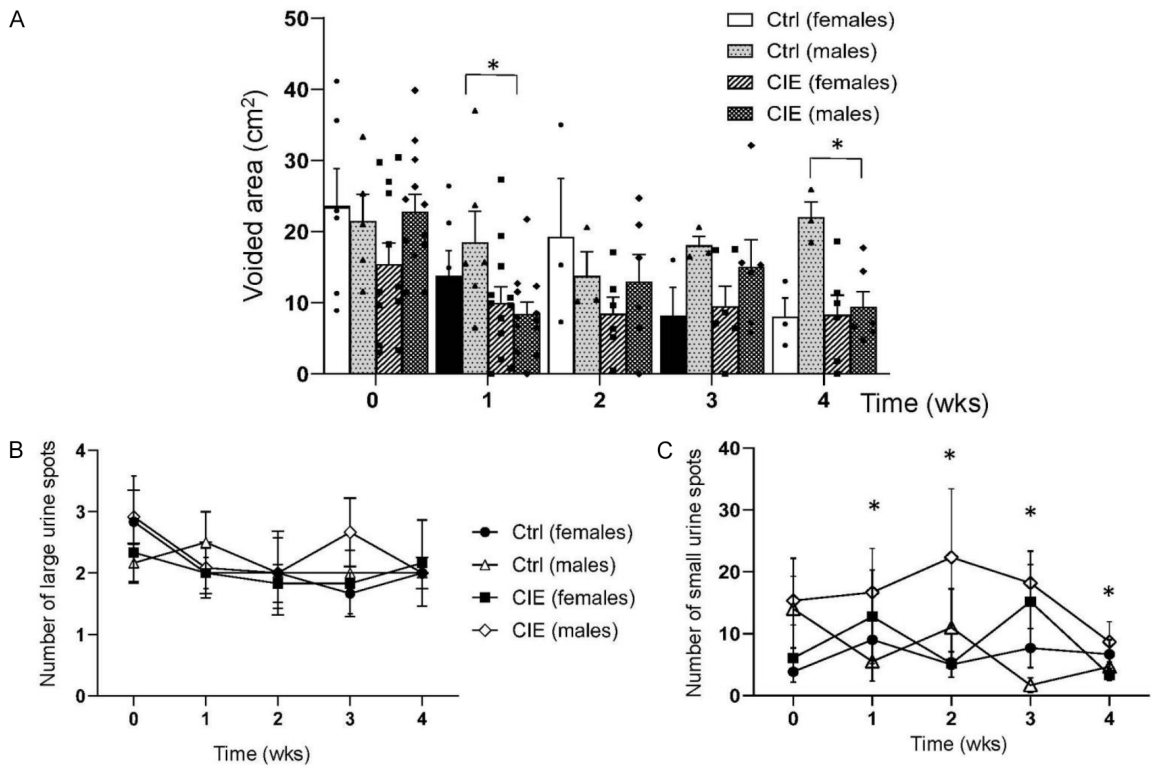

Figure 2. Voiding spot assay (VSA) analysis. A. The area distribution of all voided spots (mean ± SEM, P≤0.05 to respective control). Each dot represents a single measured/counted void (n) for all animals in that sex/group. B. Number of large urine spots (>0.5 cm^2) per each experimental group (mean ± SEM). C. Number of small urine spots (<0.5 cm^2) per sex/group (mean ± SEM; *P<0.05 to respective sex control group).

(**Figure 1D**), whereas control mice showed steady increases in body weight from 20.5±0.5 g (day 0) to 32.0±0.3 g at 4 wks (56% increase, P≤0.001, **Figure 1D**). Both groups of female CIE mice developed significant neurological impairment with the CSS reaching 2.2±0.7 (CIE, 1 wk) and 2.6±0.4 (CIE, 4 wks) at 7 days after the infection, followed by the recovery of the symptoms by 4 wks post-infection (P≤0.05 to baseline, **Figure 1E**). None of the control male or female mice developed any neurological clinical symptoms within the entire period of observation.

Analysis of voiding behavior in CIE males revealed weekly fluctuations in the volume of voided urine with a significant reduction observed at 1 wk (by 54.3%, P≤0.05 to respective control, **Figure 2A**) and 4 wks (a decrease by 57.3%, P≤0.05 to respective control group, **Figure 2A**). Female CIE mice also experienced variations in voided urine volume within the entire period of testing in both control and CIE groups, but without reaching a statistical significance (**Figure 2A**). The number of large urine spots in control and CIE mice was similar among the sexes, reaching 2-3 voids per mouse (**Figure 2B**). The number of small urine spots, usually reflective of spontaneous or uncontrolled leakage of urine, was comparable between control and CIE female groups (**Figure 2C**). Male CIE mice, however, had a significantly increased number of small urine spots starting from 1 wk post-infection (16.7±7.1 vs 5.5±3.1 in respective control group, P≤0.05) and maintained a 2-fold increase between 2 and 4 wks of observation (**Figure 2C**) suggestive of more substantial impact of neuroinflammation on bladder function in CIE males in comparison to females.

Differential baseline gene expression in LS DRG from male and female mice

The results of bulk RNAseq revealed approximately 18000 annotated genes in each group that were subjected to DESeq2 analysis. Differentially expressed genes (DEGs, fold

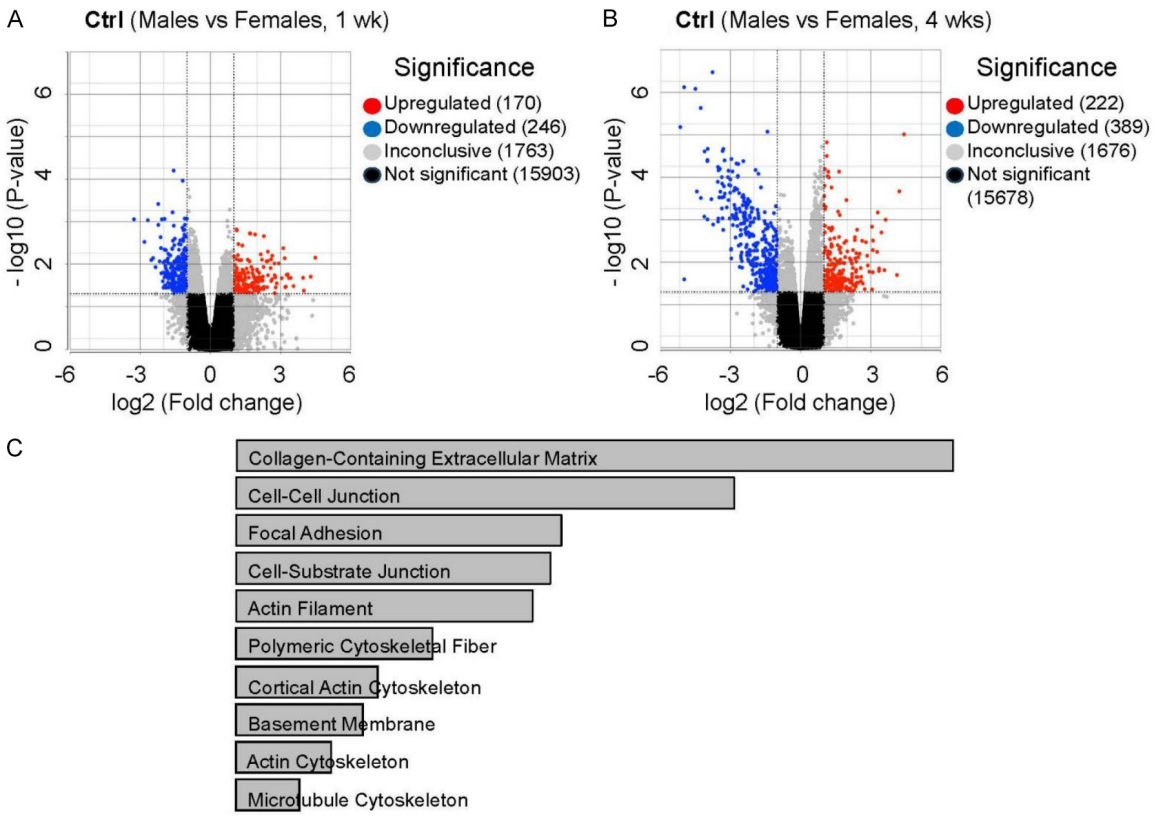

Figure 3. Comparison of gene expression between male and female mice in the control groups (1 wk and 4 wks). A. Volcano plot reflects the comparison of up- and downregulated genes in the first control group (1 wk) when males were compared to females. B. Volcano plot comparison of the genes expressed in males *vs* females in the second control group (4 wks). C. Top biological processes significantly changed in male and female control groups at 4 wks *vs* 1 wk post-infection (age-related changes).

change >1.5 and <-1.5, P≤0.05) were used to create IPA pathway networks. The comparison of transcriptomic data between control male and female mice revealed substantial differences in the number and functional type of DEGs. Volcano plot in **Figure 3A** shows that in the first control group (1 wk after saline injection) 170 genes were upregulated in male *vs* female mice and 246 genes were downregulated in males when compared to females. Gene ontology comparisons between male and female control mice (1 wk group) reveled an upregulation of the DEGs belonging to oxidative phosphorylation, protein folding, adrenergic receptor signaling, glycolysis, and PPRAα/RXRα activation in the male group. Among the downregulated genes in male *vs* female controls (1 wk) were the ones associated with IL-4 and IL-13 signaling, EGR2 and COX2-mediated myelination, extracellular matrix organization including integrins and collagen fibrils, and HEY1 pathway (data not shown).

The comparison of DEGs between sexes in the second control group (4 wks), revealed that 222 genes were upregulated and 389 genes were downregulated in males in comparison to females (**Figure 3B**). The genes upregulated in the male control group at 4 wks were related to collagen and cholesterol biosynthesis, EGR2 and COX2-mediated myelination, IGF transport, and post-translational protein phosphorylation. Ephrin 1 signaling, phagosome formation, VEGF and actin cytoskeleton signaling, and neutrophil degranulation pathways were downregulated in males in comparison to the respective control group of females (4 wks). In general, female control groups had an increased baseline leukocyte migration and neutrophil degranulation processes (immune system related), along with an upregulated extracellular matrix (ECM) reorganization and ECM-receptor interactions. The main signaling pathways which changed with age (from 1 wk to 4 wks) in age-combined male and female control groups

A

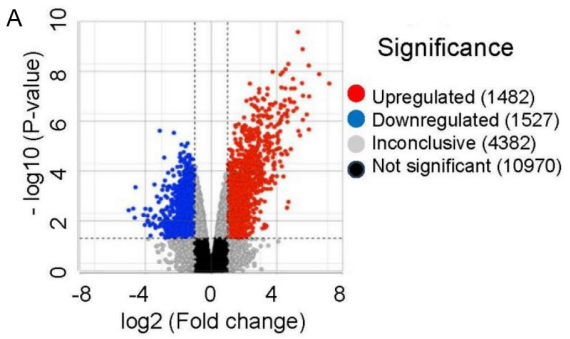

C

Upregulated genes	Fold change	Function	Location
Gm12250	145.8	Predicted gene 12250	Cytoplasm
Iigp1	95.1	Interferon inducible GTPase 1	ECS
Gbp2	62.4	Guanylate binding protein 2	Cytoplasm
Ccl5	61.6	C-C motif chemokine ligand 5	ECS
Cd8a	61.4	CD8 subunit alpha	PM
Tgtp1/Tgtp2	56.4	T cell specific GTPase 1	Other
Apol6	48.2	Apolipoprotein L6	ECS
Gbp6	47.3	Guanylate binding protein 6	Cytoplasm
Cd3e	46.3	CD3ε of T-cell receptor	PM
Bc023105	42.4	GTPase-like pseudogene	Other

B

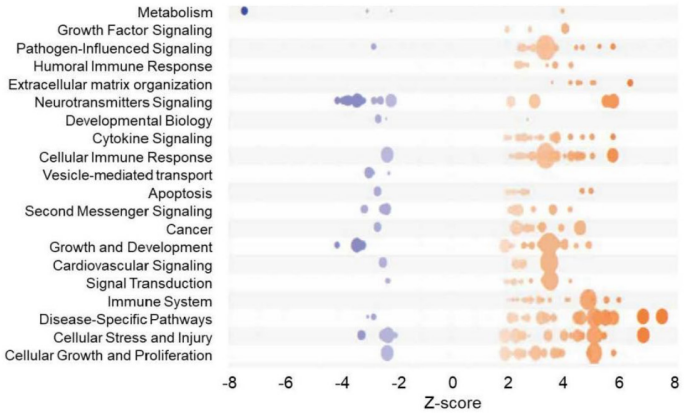

Figure 4. Bulk RNAseq data from sensory ganglia of male CIE mice (acute phase, 1 wk post-infection with the virus). A. Volcano plot of the DEGs. B. Pathway category changes in male CIE mice automatically grouped by IPA software. Blue bubbles on z scale mean significantly downregulated genes in a signaling pathway; orange bubbles reflect significantly upregulated genes in a signaling pathway, and grey bubbles reflect no significant change. The size of the bubbles reflects linear correlation with the number of genes that overlap the pathways. C. Top 10 upregulated genes in male CIE mice. ECS - Extracellular space; PM - plasma membrane; Other - outside of the cell.

included 108 DEGs that were related to ECM changes, including collagen-containing ECM, cell-cell junctions, focal adhesions, and actin and microtubule cytoskeleton reorganization (**Figure 3C**).

Effects of neuroinflammation on gene expression profiles of sensory ganglia from male CIE mice

Due to substantial sex differences in gene expression detected at the baseline, we performed separate analyses of the transcriptomic datasets in male and female groups. Viral induction of neuroinflammation in male mice triggered the most significant changes in the transcriptional profiles of DRG during the acute stage of the disease (1 wk). In comparison to age-matched control group, 3009 genes were significantly changed in CIE males with 1482 genes being up- and 1527 downregulated after the infection (**Figure 4A**). Pathway category analysis revealed the most significant upregulation of DEGs in cellular immune responses, cell injury, signal transduction, growth and development, and pathogen-associated signaling (**Figure 4B**). Downregulated pathways included genes associated with cellular growth, proliferation and development, immune responses, and nervous system signaling but with fewer genes comprising each category (**Figure 4B**). Analysis of molecular interactions and pathways determined that coronaviral infection triggered extensive immune responses involving the families of interferons (*Ifna2, Ifng, Ifnl1*), interleukins (*Il1a, Il1b, Il6*), toll-like receptors (*Tlr9, Tlr7*), and cytokines (*Ccl5)* among other upregulated DEGs. The top 10 upregulated genes in male CIE group (1 wk) have 3 members of the guanylate-binding proteins family (GTPases) that are activated by interferon (IFN)-gamma and are part of the protective immunity against bacterial and viral pathogens (**Figure 4C**). These genes included *Iigp1* (95-fold increase, encodes interferon inducible GTPase 1 protein), *Gbp2* (62-fold increase, encodes

Table 1. Top 10 downregulated genes in male CIE mice at 1 wk post-infection

Downregulated genes	*Fold change*	*Function*	*Protein Location*
Albfm1	-34.20	Albumin superfamily member 1	Other
Gm15666	-26.75	Keratin 19 pseudogene	Other
Ucp1	-25.15	Uncoupling protein 1	Cytoplasm
Gm31816	-24.33	Predicted gene 31816	Other
Nhlh1	-17.36	Nescient helix-loop-helix 1	Nucleus
Scgn	-16.41	Secretagogin, Ca^{2+} binding protein	Cytoplasm
Gm19076	-16.0	Proteasome β1 pseudogene	Other
Tdrd1	-14.58	Tudor domain containing 1	Cytoplasm
Rag1	-14.27	Recombination activating 1	Nucleus
Ccdc175	-14.15	Coiled-coil domain containing 175	Other

guanylate binding protein 2), and *Gbp6* (46-fold increase, encodes guanylate binding protein 6). The second group in top 10 upregulated genes was associated with T cells and included *Cd8a* (61-fold increase, encodes CD8 subunit alpha), *Tgtp1/Tgtp2* (56-fold increase, encodes T cell specific GTPase 1) and *Cd3ε* (46-fold increase, encodes Cd3ε subunit of T-cell receptor). Among the top 10 downregulated genes were a member of the albumin family (*Albfm1*, 34-fold decrease), the *Ucp1* gene encoding a mitochondrial protein (25-fold decrease), and the *Scng* gene encoding Ca^{2+}-binding protein secretagogin (16-fold decrease, **Table 1**).

In comparison to the acute phase of neurodegeneration (1 wk), the transcriptomic profile of DRG in CIE males at 4 wk (beginning of demyelination in the CNS) revealed a 6-fold decrease in the number of DEGs (510 *vs* 3009 at 1 wk) with 353 genes being up- and 157 down-regulated after the infection (**Figure 5A**). Among all DEGs, 242 overlapped with the 1 wk time point (**Figure 5B**). Pathway category changes analysis revealed the most significant upregulation of the genes in the immune system, cellular immune responses, cellular stress and injury, growth/proliferation and development, and pathogen-associated signaling pathways, which were similar to the pathways upregulated in CIE (1 wk) group (**Figure 5C**). Downregulated pathways included genes associated with intracellular and second messenger signaling, disease-specific pathways, neurotransmitters/nervous system signaling, and ingenuity toxicity (**Figure 5C**). The list of top 20 DEGs (10 up- and 10 downregulated) for the second male CIE group (4 wks) is included in **Table 2**. The top 10 upregulated genes in male CIE group (4 wks) included 2 members of the immunoglobulin family (*Ighg2b*, 41-fold increase and *Igha*, 10-fold increase), 2 myosin-related genes (*Myh2*, 8-fold, encodes myosin heavy chain 2 and *Mybpc1*, 7-fold increase, encodes myosin binding protein C1), *Gad1* (14-fold increase, encodes glutamate decarboxylase 1), *Cfap 65* (15-fold increase, encodes cilia and flagella protein 65), *Ly6a* (10-fold increase, encodes lymphocyte antigen 6a), and *Ccr1* (9-fold increase, encodes C-C motif chemokine receptor 1). The list of downregulated genes included 2 protamine-encoding genes (*Prm1*, 12-fold decrease and *Prm2*, 10-fold decrease), *Ssmem1* (10-fold decrease, encodes serine rich membrane protein 1), *Crisp2* (9-fold decrease, encodes cysteine rich secretory protein 2), *Tnp2* (9-fold decrease, encodes transition protein 2), and *Cabs1* (9-fold decrease, encodes calcium binding protein).

Short- and long-term transcriptomic changes in DRG of female CIE mice

Gene expression analysis of sensory ganglia from female CIE mice revealed 481 DEGs in comparison to the age-matched control group with 275 genes being up- and 206 downregulated after the infection (**Figure 6A**). Similar to the male CIE group, the top 10 up-regulated genes in female CIE mice (1 wk) include 3 members of the guanylate-binding proteins family (GTPases) - *Gbp3* (88-fold increase, encodes guanylate binding protein 3), *Gbp8* (31-fold increase, encodes guanylate binding protein 8), and *Iigp1* (30-fold increase, encodes interferon inducible GTPase 1 protein, **Figure 6B**). In addition, upregulated genes also included two T-cell associated genes: *Icos* (36-fold increase,

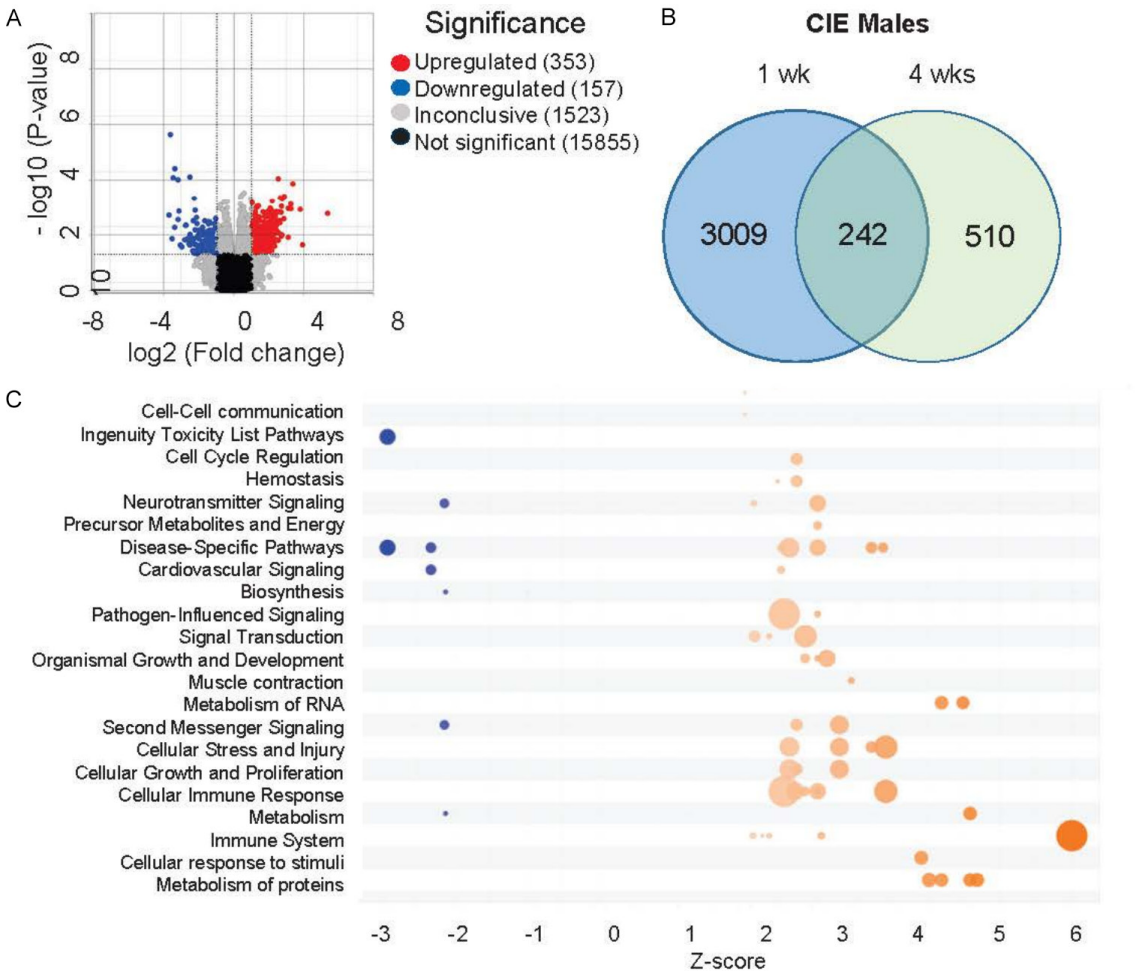

Figure 5. Transcriptomic changes in male CIE mice at 4 wks post-inoculation with the virus. A. Volcano plot of the DEGs. B. Venn diagram reflects the comparison of gene expression in CIE males between 1 and 4 wks. 242 significantly changed genes overlap between CIE males at 1 wk *vs* 4 wks. C. Pathway category changes in male mice. Blue bubbles on z scale mean significantly downregulated genes in a signaling pathway; orange bubbles reflect significantly upregulated genes in a signaling pathway. The size of the bubbles reflects linear correlation with the number of the genes that overlap the pathways.

encodes inducible T cell co-stimulator) and *Cd8a* (33-fold increase, encodes CD8 subunit alpha), as well as *Gzmb* gene (175-fold increase, encodes Granzyme B), *Il12rb1* gene (56-fold increase, encodes IL12 subunit beta-1), and *Cxcl9* gene (60-fold increase, encodes C-X-C motif chemokine ligand 9). The upregulated genes in the female CIE group (1 wk) belong to a limited number of signaling pathways including immune responses, cellular stress and injury, pathogen-associated signaling pathways, and apoptosis (**Figure 6C**). Most of the top 10 downregulated genes in female CIE mice (1 wk) were pseudogenes with undefined function (*Gm6724, Gm13274, Gm24514, Gm35065, Gm37626 etc)* except for *Prm2* (11-fold decrease), which encodes Protamine 2 (**Table 3**). However, the rest of downregulated genes and associated pathways were more diverse than the upregulated ones and included genes belonging to neurotransmitters and nervous system signaling, cellular growth, proliferation, and development, cellular immune responses, pathogen-associated signaling, and second messenger pathways (**Figure 6C**).

The analysis of transcriptomic profiles of LS DRG in CIE females at 4 wks revealed a 2-fold decrease in the total number of DEGs (264 *vs* 481 at 1 wk) with 106 genes being up- and 158

Table 2. Top 10 up- and downregulated genes in male CIE mice at 4 wk post-infection

Upregulated genes	*Fold change*	*Function*	*Protein Location*
Ighg2b	41.40	Immunoglobulin heavy γ 2B	Extracellular Space
Cfap65	15.25	Cilia and flagella protein 65	Cytoplasm
Gad1	13.89	Glutamate decarboxylase 1	Cytoplasm
Igha	10.36	Immunoglobulin heavy α	Plasma Membrane
Lmod2	9.61	Leiomodin 2	Other
Ly6a	9.57	Lymphocyte antigen 6A	Plasma Membrane
Ccr1	8.61	C-C motif chemokine receptor 1	Plasma Membrane
Myh2	8.60	Myosin heavy chain 2	Cytoplasm
Atcayos	7.39	Ataxia, cerebellar, opposite strand	Other
Mybpc1	7.25	Myosin binding protein C1	Cytoplasm
Downregulated genes			
Prm1	-12.23	Protamine 1	Nucleus
Ldhc	-10.93	Lactate dehydrogenase C	Cytoplasm
Ssmem1	-10.31	Serine rich membrane protein 1	Other
Prm2	-10.24	Protamine 2	Nucleus
Tnp2	-9.01	Transition protein 2	Nucleus
Cabs1	-8.98	Calcium binding protein	Extracellular Space
Crisp2	-8.68	Cysteine rich secretory protein 2	Extracellular Space
Tcp11	-8.22	T-complex 11	Cytoplasm
Spmip9	-7.73	Sperm microtubule inner protein 9	Cytoplasm
Folr2	-6.53	Folate receptor beta	Plasma Membrane

downregulated after the infection (**Figure 7A**). Among all DEGs, 40 overlapped with the 1 wk time point (**Figure 7B**). Pathway category analysis revealed the most significant upregulation of the genes in the disease-specific pathways, transcriptional regulation, cellular growth, proliferation and development, and second messenger signaling (**Figure 7C**). The downregulated pathways were presented more broadly and comprised the same cellular signaling categories as upregulated genes with an addition of metabolic regulation and ECM organization (**Figure 7C**). The list of top 20 DEGs (10 up- and 10 downregulated) for the second female CIE group (4 wks) is included in **Table 4**. The top 10 up-regulated genes included mostly pseudogenes except for the *Adig* gene (5.6-fold increase, encodes adipogenin), and *Sucnr1* (6-fold increase, encodes succinate receptor 1). The top 10 downregulated genes in female CIE mice (4 wks) consisted of 6 gene members encoding motor proteins. They included myosin heavy (*Myh7*, 21-fold decrease, encodes myosin heavy chain 7) and light chain (*Myl2* and *Myl3,* 9-fold decrease for both) genes, as well as troponins (*Tnnt1* and *TnnI1*), and dynein (*Dnah5*) encoding genes. *Igha* and *Nmrk2* (7-fold decrease for each) were also among the top 10 downregulated genes encoding immunoglobulin heavy constant α and nicotinamide riboside kinase 2, respectively.

Comparison of male and female transcriptomic profiles during early and late stages of neurodegeneration

Next, we compared the transcriptomic datasets of male and female CIE groups at earlier (1 wk) and later (4 wks) stages of neurodegeneration. During the acute stage of neuroinflammation in the CNS (1 wk), 343 genes were significantly changed between male and female groups (**Figure 8A**). In the top 25 DEGs, the genes upregulated in both sexes included *Cd8a, Cd3g, Ms4a4b, Gbp2, Gbp3, Gbp4, Igtp, Tgtp1, Zbp1,* and *Ccr5* among others. The genes down-regulated in both male and female groups at 1 wk post-infection included *Vpreb3*, *Mrgpra2b,* and *Smr2* in addition to several poorly annotated protein-coding genes (*Gm-24514* and similar). Among the functional pathways, the 5 most significantly changed ones included inflammatory and immune responses, cellular development, growth and proliferation,

A

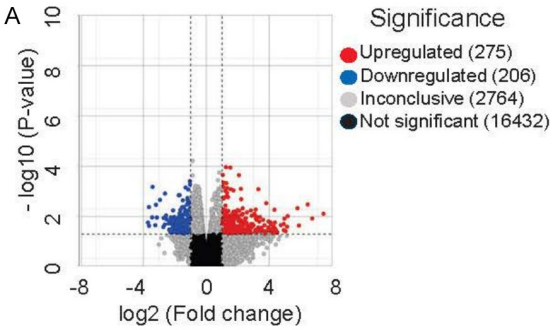

B

Upregulated genes	Fold change	Function	Location
Gzmb	176.0	Granzyme B	Cytoplasm
Gm4841	106.6	Predicted gene 4841	Other
Gbp3	87.7	Guanylate binding protein 3	Cytoplasm
Cxcl9	59.6	C-X-C motif chemokine ligand 9	ECS
IL12RB1	55.7	Interleukin 12 subunit beta 1	PM
ICOS	36.2	Inducible T cell co-stimulator	PM
Gm12250	35.3	Predicted gene 12250	Cytoplasm
Cd8A	33.0	CD8 subunit alpha	PM
Gbp8	31.3	Guanylate-binding protein 8	Other
Iigp1	30.5	Interferon inducible GTPase 1	ECS

C

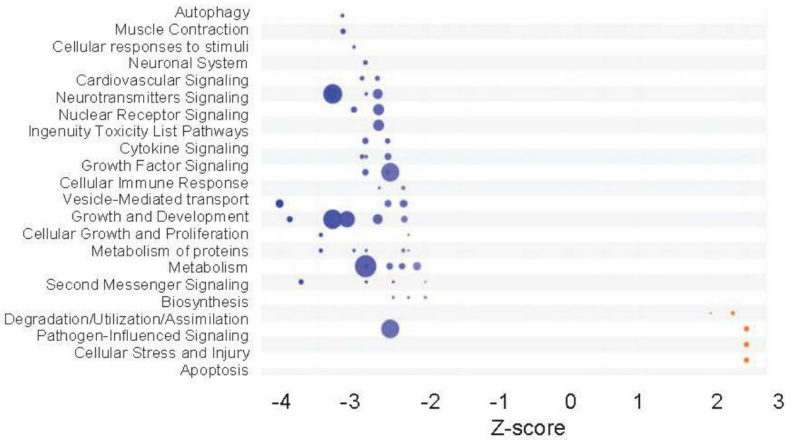

Figure 6. Analysis of gene expression in LS sensory ganglia of female CIE mice at early stage of neuroinflammation (1 wk). A. Volcano plot of DEGs. B. The table of top 10 upregulated genes in female CIE mice at 1 wk. ECS - Extracellular space, PM - plasma membrane, Other - outside of the cell. C. Pathway category changes in female mice during acute stage of neuroinflammation in the CNS caused by a coronavirus. Blue bubbles on z scale mean significantly downregulated genes in a signaling pathway; orange bubbles reflect significantly upregulated genes in a signaling pathway. The size of the bubbles reflects linear correlation with the number of the genes that overlap the pathways.

Table 3. Top 10 downregulated genes in female CIE mice at 1 wk post-infection

Downregulated genes	*Fold change*	*Function*	*Protein Location*
Gm6724	-13.05	High mobility group pseudogene	Other
Gm13274	-12.56	Predicted gene 13274	Other
Gm24514	-12.50	n/a	Other
Gm35065	-10.87	n/a	Other
Prm2	-10.70	Protamine 2	Nucleus
Gm37626	-9.48	n/a	Other
Gm8770	-9.20	protein 8 pseudogene	Other
Gm47629	-8.84	Predicted gene, 47629	Other
Gm18305	-8.13	Antigen 2 pseudogene	Other
Gm38150	-7.71	n/a	Other

cellular movement, cell death and survival, and organismal injuries/abnormalities (**Figure 8B**).

During the demyelination stage (4 wks post-infection), the number of overlapping genes was reduced to 81 between CIE males and females (**Figure 8C**). However, among the upregulated genes, only *Ube2nl* overlapped between male and female groups, whereas among downregulated genes, the overlapping genes included *Tnp2, Efcab6,* and *Gm4335*. The comparison of DEGs at both time points revealed the predominant number of upregulated genes in CIE males (**Figure 9**). The upregulated genes belonged to the neutrophil degranulation pathway, cytokine storm signaling, MS

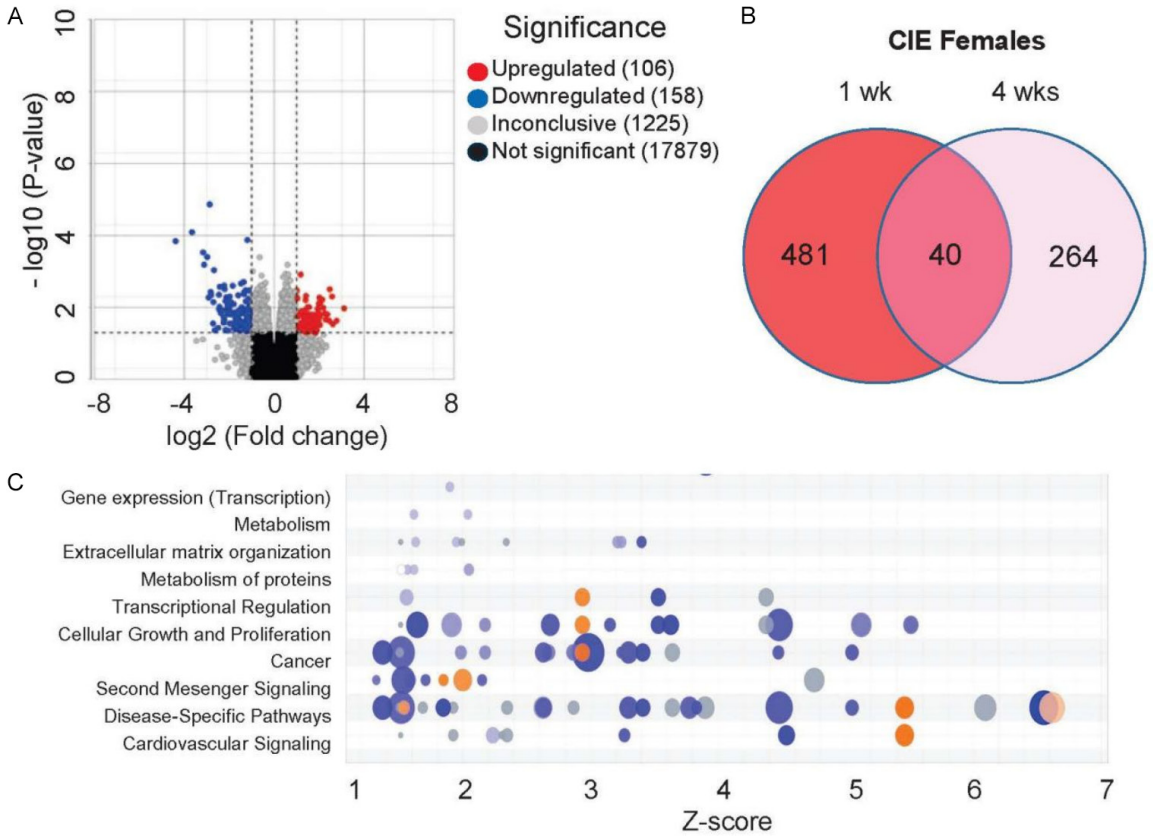

Figure 7. Transcriptomic data from sensory ganglia of female CIE mice at later stage of neurodegeneration. A. Volcano plot of the DEGs. B. Venn diagram shows the comparison of gene expression in female CIE mice between 1 and 4 wks. 40 DEGs overlap in CIE females at 1 wk *vs* 4 wks. C. Pathway category changes in female mice grouped by cellular processes. Blue bubbles on z scale mean significantly downregulated genes in a signaling pathway; orange bubbles reflect significantly upregulated genes in a signaling pathway. The size of the bubbles reflects linear correlation with the number of the genes that overlap the pathways.

signaling, neuroinflammation and Th1 pathways, dendritic maturation, IFN-γ signaling, and macrophage classical activation signaling among the others (**Figure 9**). In females, however, the number of upregulated DEGs was much lower at 1 wk, and most of the DEGs at 4 wks were down-regulated (**Figure 9**). Among the pathways upregulated in males but downregulated in females at both time points were the phagosome formation pathway, neutrophil extracellular trap signaling, hepatic fibrosis signaling, and the oxytocin pathway. The downregulation of the DEGs in these signaling pathways was more prominent at 4 wks post-infection (**Figure 9**).

Discussion

Neurogenic LUTS in MS patients are well documented and usually linked to ongoing neuroinflammatory and neurodegenerative changes in the CNS [20]. Many symptoms include alterations in LUT sensation (urgency, overactivity, incomplete emptying *etc*) processed by bladder sensory neurons residing within DRG. Unlike in the gastrointestinal tract, the UB lacks intrinsic neurons within the bladder wall, therefore, DRG neurons are the first ones to receive afferent input from the LUT before transmitting this information to the spinal cord and brain [6]. Alterations in LUT sensation in MS patients suggest potential functional changes in excitability of sensory neurons and/or function of surrounding satellite glia and other intraganglionic cell types. Patients suffering from MS-related sensory dysfunction experience a significantly diminished quality of life [20]. Therefore, in the current study, we assessed the transcriptomic profile of the LS sensory ganglia receiving afferent input from the LUT and clarified the role of sensory interoception in the DRG-urinary bladder crosstalk in a sex-biased manner.

Table 4. Top 10 up- and downregulated genes in female CIE mice at 4 wk post-infection

Upregulated genes	*Fold change*	*Function*	*Protein Location*
Gm12341	8.643	Predicted gene 12341	Other
C19orf81	6.883	Chromosome 19, frame 81	Other
Gm15495	6.11	Chaperonin Tcp1 pseudogene	Other
Sucnr1	5.964	Succinate receptor 1	Plasma Membrane
Adig	5.563	Adipogenin	Cytoplasm
Gm36944	5.457	n/a	Other
4921514A10Rik	5.152	RIKEN cDNA 4921514A10 gene	Other
Gm47333	4.964	n/a	Other
Gm10644	4.954	Predicted gene 10644	Other
Rp23-350f7.3	4.88	n/a	Other
Downregulated genes			
Myh7	-20.90	Myosin heavy chain 7	Cytoplasm
Tnnt1	-12.60	Troponin T1, slow skeletal type	Cytoplasm
Cfap65	-11.02	Cilia and flagella protein 65	Cytoplasm
Sox1	-9.02	SRY-box transcription factor 1	Nucleus
Myl2	-8.94	Myosin light chain 2	Cytoplasm
Myl3	-8.66	Myosin light chain 3	Cytoplasm
Tnni1	-7.85	Troponin I1, slow skeletal type	Cytoplasm
Dnah5	-7.55	Dynein axonemal heavy chain 5	Cytoplasm
Igha	-7.29	Immunoglobulin heavy constant α	Plasma Membrane
Nmrk2	-7.09	Nicotinamide riboside kinase 2	Plasma Membrane

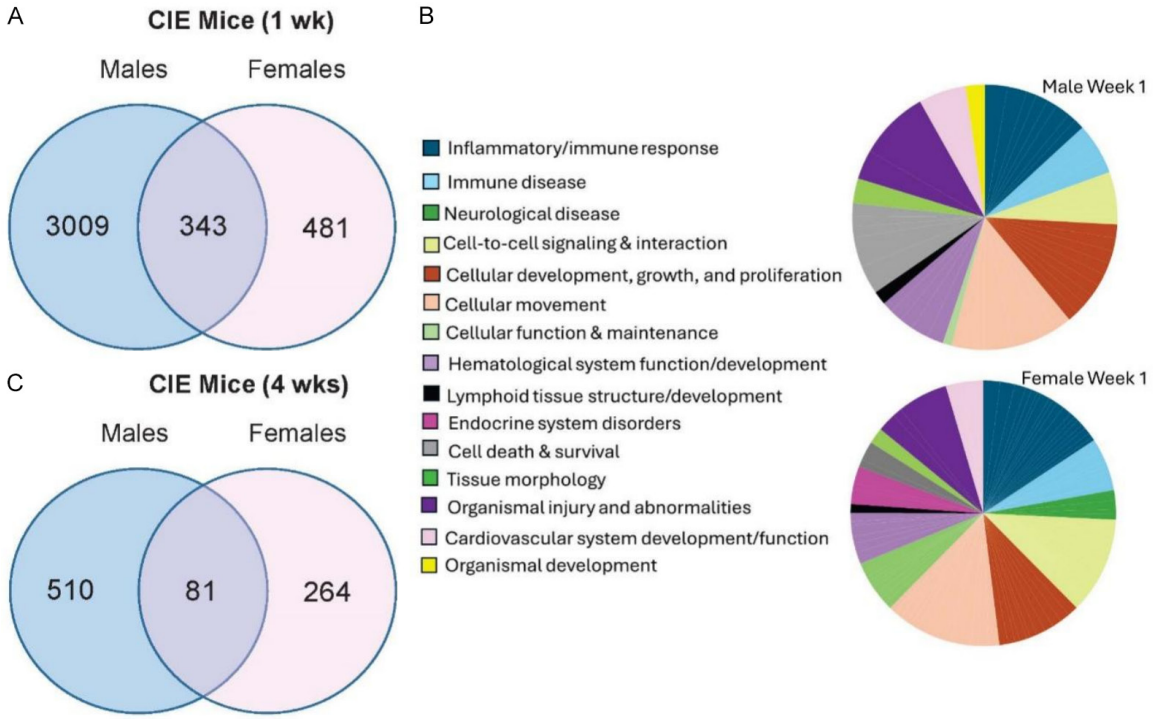

Figure 8. Time-dependent comparison of gene expression between male and female CIE groups. A. 343 significantly changed genes overlap between CIE males and females at 1 wk post-inoculation. B. 81 significantly changed genes overlap between CIE males and females at 4 wks time point. C. DEGs functions grouped into related pathways. Proportions were determined by the number of genes in our dataset divided by the number of genes within a pathway.

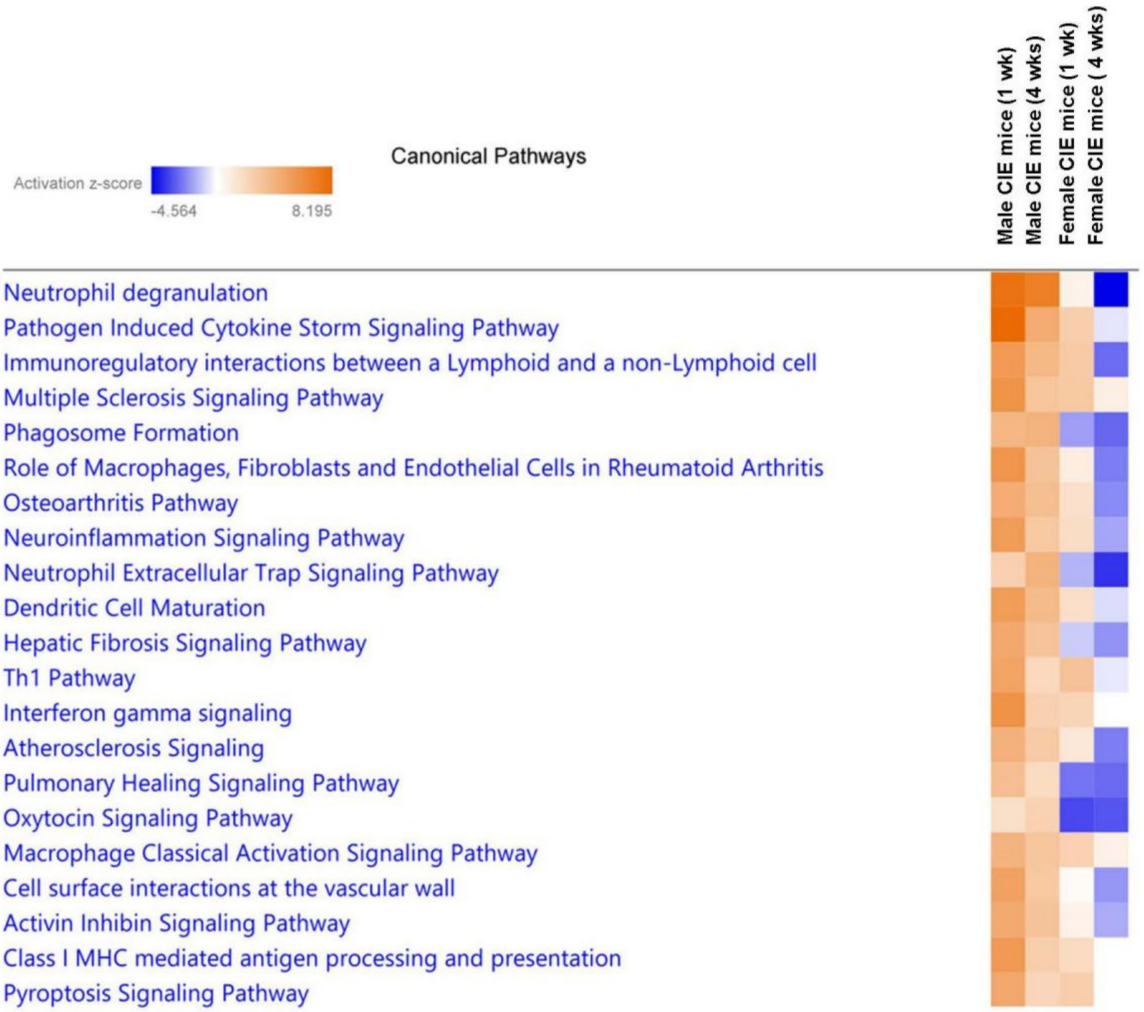

Figure 9. DEGs grouped by canonical pathways for male and female CIE groups. Z score reflects the fold changes in down- (blue) and upregulation (orange) for each pathway.

The analysis of transcriptomic profiles of LS DRG from control mice confirmed sex specific differences in DEGs of males and females at the baseline. In general, female control groups showed an increased expression of genes involved in leukocyte migration and neutrophil degranulation processes (immune system related) along with an upregulated extracellular matrix (ECM) reorganization and ECM-receptor interactions. In comparison, control males showed an elevated expression of the genes belonging to oxidative phosphorylation, protein folding, adrenergic receptor signaling, collagen and cholesterol biosynthesis, IGF transport, and posttranslational protein phosphorylation. Sexual dimorphism in gene expression profiles of sensory ganglia has been previously reported in naïve animal [12, 36] and human DRG [37, 38]. Our data also correlate with previously published studies that identified activated immune pathways in females in comparison to males at the baseline [39]. *Sorge et al.* reported a prominent sex dimorphism when studying mechanical hypersensitivity. In males, mechanical responses were associated with activation of microglial pathways, whereas in females, they were dependent on adaptive immune responses [38, 40]. Baseline differences in DRG gene expression across sexes could be influenced by several factors. First, the role of gonadal hormones during development is well established and plays a prominent role in gene and protein expression of many cellular targets [41]. Second, sex differences could also arise as a consequence of the sex chromosome complement action (XX and XY) [42, 43]. Previous

studies established that sex chromosomes play a role in glucose homeostasis, fatty liver, adiposity, and feeding behavior independently of the action of sex hormones [44, 45]. Third, heterogeneity of the cells within a single DRG could contribute to transcriptomic sex differences due to different cell types being unequally affected by gonadal hormones. Only a small proportion of DRG cells are neurons with the remaining cells being non-neuronal [46]. Therefore, RNAseq data from the whole DRG reflects a strong influence of non-neuronal cells on the transcriptome. Fourth, several pelvic organs innervated by LS DRG (*e.g.* UB, distal colon, male and female reproductive tracts) may have specific crosstalk influences on neuronal and glial phenotypes within DRG leading to heterogeneity in DEGs. Finally, preparation methods of DRG isolation and total RNA extraction could also potentially impact the RNAseq outcomes.

Our results confirmed that a coronaviral infection of mice led to the development of significant acute (at 1 wk) and chronic (at 4 wks) neuroinflammation in animals of both sexes. Our prior studies determined that male mice inoculated with MHV developed acute inflammation in the CNS followed by progressive demyelination [31, 32]. They also presented with a significant neurologic deficit associated with voiding dysfunction that was comparable with neurogenic LUTS observed in MS patients [33]. In the present study, we observed a more prominent impact of CNS neuroinflammation on voiding patterns in CIE males in comparison to females. The male CIE group had an increased number of small voiding spots during acute stage of neuroinflammation with similar CSS recorded in both groups, followed by a recovery from neurological symptoms at 4 wks post-inoculation. Infection with the virus triggered extensive immune responses in CIE males during acute phase including an upregulation of the family of interferons (*Ifna2, Ifng, Ifnl1*), interleukins (*Il1a, Il1b, Il6*), toll-like receptors (*Tlr9, Tlr7*), and chemokines (*Ccl5).* Interferons (IFNs) are a family of proteins with immunomodulating properties that have been detected in active MS lesions [47]. IFN-β was the first approved therapy for MS patients [48] with favorable long-term safety profiles [49]. Interleukins are the major regulators of the immune system among the cytokines and have a major influence on immune-mediated diseases. Interleukins IL-1, IL-3, IL-4, IL-6, IL-10 and IL-12 are associated with substantial immune responses such as excessive inflammation, loss of immune tolerance, altered T-cell differentiation, and inflammatory cell recruitment [50]. Toll-like receptors (TLRs) are also directly involved in the regulation of inflammatory reactions. The role of TLR activation in the development of MS has been widely studied in MS patients and several murine models of MS [51]. *Trl7* is expressed in monocytes and macrophages, plasmacytoid dendritic cells and B cells, and TRL7 binds to single-stranded (viral) RNA [52]. Some MS patients express elevated mRNA levels of TLR7 at the onset of the disease, suggesting an early involvement of this receptor in the pathogenesis of MS development [53]. Animal studies using experimental autoimmune encephalomyelitis (EAE) model of MS confirmed that TLR7 agonists provide more effective results when used in combination with other drugs. Suppression of EAE with TLR7 agonist correlated with a significant decrease in the infiltration of monocytes, granulocytes, and natural killer (NK) cells, reduced demyelination, and downregulation of *IL-1β*, *Ccl2*, and *Ifnγ* gene expression in the spinal cord of EAE mice [54]. Cytokines are another group of signaling proteins that regulate inflammation and other cellular activities including chemokines that specialize in cell migration. CCL5 is one of the chemokines involved in the pathophysiology of MS as they accumulate in active lesions, and are expressed by resident glia and perivascular leukocytes in human MS [55-57]. Specifically, CCL5 functions as a chemoattractant for circulating monocytes, T helper cells, and eosinophils. It can also trigger the recruitment of leukocytes into inflammatory sites and stimulate activation of NK cells [58]. In our previous study [59], we determined there to be an upregulation of *Ccl5* expression in the spinal cord of CIE mice. Other studies detected CCL5 at increased levels in the urine of patients with bladder pain syndrome that presented with voiding dysfunction and LUTS [60, 61]

Analysis of upregulated DEGs in sensory ganglia of male and female CIE groups (at 1 wk) revealed several genes belonging to GTPase members of the guanylate-binding proteins (GBP) family (in males - *Iigp1, Gbp2 and Gbp6* genes; in females - *Iigp1, Gbp3* and *Gbp8).* Our

results correlate with previously published transciptomic data from human MS specimens and animal models. GTPases of the GBP family are activated by interferon (IFN)-gamma, and are known as part of “guard immunity” against bacterial and viral pathogens [62, 63]. Clinical studies focused on DEGs in the serum of MS patients identified *GBP2* as one of the genes for predicting relapse-free survival in MS patients [64]. GBP1 is the most characterized member of the GBP family, and was determined to be one of key biomarkers in the lesioned grey matter of patients with secondary progressive MS [65]. Animal studies using EAE and cuprizone (CPZ) models of MS found interferon-inducible GTPase 1 (*Iigp1*) to be in the top 5 highly expressed genes in the sensory cortex of EAE-treated mice [66], in addition to an upregulated expression of *Gbp6* and *Ccl12* in the brains of both EAE and cuprizone-treated mice [66]. It must be noted that an upregulation of the DEGs encoding chemokines, chemokine-ligands, and GBPs has been recorded on all animal models of MS (EAE, CIE and CPZ) with some variability between the top 10 DEGs [66].

The second group of top 10 upregulated genes in DRG of both male and female CIE mice during acute stage of coronavirus-induced neuroinflammation was related to immune cells, including T cells and these associated receptors: *Cd8a* (61-fold increase in males, 33-fold increase in females), *Tgtp1/Tgtp2* (56-fold increase in males, encodes T cell specific GTPase 1), *Cd3ε* genes (46-fold increase in males, encodes Cd3ε subunit of T-cell receptor), *Il12rb1* gene (56-fold increase in females, encodes IL12 subunit beta-1), and *Cxcl9* gene (60-fold increase in females, encodes C-X-C motif chemokine ligand 9). We previously reported a significant upregulation of the same group of DEGs in the spinal cord of male CIE mice [59]. *Cd8a* gene ecodes a protein that mediates cell-to-cell interactions within the immune system, and is expressed by cytotoxic T lymphocytes [67]. *Cd3ε* gene encodes the protein which is part of the CD3 T-cell receptor, along with other subunits *Cd3e* and *Cd3d* shown to be important for antigen recognition [68].

There was a limited number of the same down-regulated DEGs in top 10 group between CIE males and females at 1 wk post-infection including only 3 overlapping genes - *Vpreb3*, *Mrgpra2b* and *Smr2* - in addition to several poorly annotated protein-coding genes (*Gm24-514 etc*). *Vpreb3* gene encodes a protein involved in B lymphocyte differentiation, and was found to be significantly upregulated in the brain of young (6 wks of age) but not old (8-15 months) mice in the EAE model of MS [69]. *Mrgpra2b* gene encodes a murine ortholog of Mas-related G-protein coupled receptors (MRGPR) family that is mainly expressed by DRG neurons and specialized immune cells [70]. The *Mrgpr* gene family includes more than 50 members in rodents and humans with many of them encoding orphan receptors with unknown ligands and physiological roles [70]. In relation to sensory ganglia, MRGPRD is often used as a marker of non-peptidergic nociceptors [46], whereas MRGPRX2 was found to be expressed in sensory neurons, mast cells and, most recently, keratinocytes [71]. The third gene found to be downregulated in both male and female CIE groups, *Smr2,* encodes murine submaxillary gland androgen regulated protein 2, suggested to be involved in regulation of sensory perception of pain and activation of endopeptidase inhibitory activity [72]. It is expressed in a subpopulation of calcitonin-G-related peptide (CGRP+, peptidergic) DRG neurons that give rise to lightly myelinated Aδ caliber axons [73]. $SMR2^+$ neurons exhibited the highest force thresholds, responding primarily to forces greater than 40 mN, and also showed responses to heat and/or cold [73].

Analyses of transcriptomic changes in DRG of male CIE mice during the chronic stage of neuroinflammation (4 wks post-infection) revealed a significant recovery of cellular processes from the initial insult as evident by a 6-fold reduction in the number of upregulated DEGs. The top 10 upregulated genes in this CIE group included 2 members of the immunoglobulin family (*Ighg2b* and *Igha)*, 2 myosin-related genes (*Myh2* and *Mybpc1*), and immune cell related genes (*Cfap 65, Ly6a* and *Ccr1).* However, only 2 genes were upregulated in CIE females at 4 wks - *Adig* and *Sucnr1*. *Adig* gene encodes adipogenin, a potent regulator of adipogenesis with a possible role in leptin regulation [74]. Overexpression of *Adig* in adipocytes substantially increased fat mass, and also elevated thermogenesis during cold exposure reflective of higher cold tolerance [75]. No pub-

lications addressed the role of adipogenin in any neurodegenerative disorders. The second gene, *Sucnr1,* encodes succinate receptor 1. Succinate is a metabolite that is released by inflammatory mononuclear phagocytes and binds to succinate receptor 1 (SUCNR1) on neural cells leading them to secrete prostaglandin E2 and scavenge extracellular succinate with consequential anti-inflammatory effects [76]. Another study confirmed that type I inflammatory mononuclear phagocytes release succinate and upregulate Sucnr1 to enhance IL-1B production in chronic inflammatory disorders such as progressive MS [77].

The downregulated pathways were presented more broadly in the chronic female CIE group (4 wks) and comprised the same cellular signaling categories identified during the acute stage including 6 DEGs that encode motor proteins - myosin heavy (*Myh7*) and light chain (*Myl2* and *Myl3*) genes, as well as troponins (*Tnnt1* and *TnnI1*), and dynein (*Dnah5*) encoding genes. The comparison of all DEGs between males and females in chronic CIE group (4 wks) revealed only one gene, *Ube2nl,* to be upregulated in both sexes, whereas in the group of downregulated DEGs, overlapping genes included *Tnp2, Efcab6,* and *Gm4335*. *Ube2nl* gene encodes putative ubiquitin-conjugating enzyme E2 N-like protein with unclear function. Proteins conjugated by ubiquitin are usually marked for degradation by proteasomes [78]. Functional studies provided evidence that several genes of the ubiquitin pathway affected regulation of neurite development, synapse formation, and pre/post synaptic function [79]. *Ube2nl* was found to be among the genes on X chromosome showing single nucleotide variants in sporadic Alzheimer's patients, and was believed to be related to respective pathology [80]. *Tnp2* was found to be downregulated in the testes of male mice in the EAE model of neurodegeneration after pregnant females were exposed to bisphenol A [81]. *Efcab6* gene, encoding a protein that binds to androgen receptors in the cells, was significantly upregulated in primary cultured astrocytes after lipopolysaccharide induced neuroinflammation [82]. In addition, *Efcab6* expression was detected in male mouse nodose/jugular ganglia with little expression in T10-L1 and L3-L5 DRGs [83].

In summary, we confirmed sex-dimorphic transcriptome changes in LS DRG in a coronavirus-induced murine model of MS characterized by the development of neurogenic LUTS. The analyses of transcriptomic datasets confirmed that virus-induced neuroinflammation in the CNS causes long-term modulation of gene expression in neurons and non-neuronal cell types within sensory ganglia. The associated changes could contribute to the development of neurogenic LUTS including altered sensations of bladder fullness, urgency, and/or pain. Further studies are warranted to address the functional role of the identified genes in neurogenic LUTS. Better understanding of the cellular pathways triggering dysfunctional voiding in male and female MS patients, as well as identification of DRG specific molecular targets would provide a necessary knowledge foundation for the development of new therapies to alleviate neurogenic LUTS in patients with neurodegenerative diseases.

Acknowledgements

We are thankful to Dr. Susan Weiss laboratory from the University of Pennsylvania for providing R59 MHV virus. This work was supported by the NIH/NIDDK grant R01 DK116648 (to APM).

Disclosure of conflict of interest

None.

Address correspondence to: Dr. Anna P Malykhina, Division of Urology, Department of Surgery, University of Colorado School of Medicine, 12700 East 19th Ave., Aurora, CO 80045, USA. Tel: 303-724-6300; E-mail: anna.malykhina@cuanschutz.edu

References

[1] Fowler CJ. The cause and management of bladder, sexual and bowel symptoms in multiple sclerosis. Baillieres Clin Neurol 1997; 6: 447-466.

[2] Fernandez O. Mechanisms and current treatments of urogenital dysfunction in multiple sclerosis. J Neurol 2002; 249: 1-8.

[3] Miller H, Simpson CA and Yeates WK. Bladder dysfunction in multiple sclerosis. Br Med J 1965; 1: 1265-1269.

[4] Fowler CJ, Panicker JN, Drake M, Harris C, Harrison SC, Kirby M, Lucas M, Macleod N, Mangnall J, North A, Porter B, Reid S, Russell N, Watkiss K and Wells M. A UK consensus on

the management of the bladder in multiple sclerosis. Postgrad Med J 2009; 85: 552-559.
[5] Tornic J and Panicker JN. The management of lower urinary tract dysfunction in multiple sclerosis. Curr Neurol Neurosci Rep 2018; 18: 54.
[6] de Groat WC, Griffiths D and Yoshimura N. Neural control of the lower urinary tract. Compr Physiol 2015; 5: 327-396.
[7] Haberberger RV, Kuramatilake J, Barry CM and Matusica D. Ultrastructure of dorsal root ganglia. Cell Tissue Res 2023; 393: 17-36.
[8] Meltzer S, Santiago C, Sharma N and Ginty DD. The cellular and molecular basis of somatosensory neuron development. Neuron 2021; 109: 3736-3757.
[9] Pan B, Zhang Z, Chao D and Hogan QH. Dorsal root ganglion field stimulation prevents inflammation and joint damage in a rat model of rheumatoid arthritis. Neuromodulation 2018; 21: 247-253.
[10] Rabiller L, Labit E, Guissard C, Gilardi S, Guiard BP, Mouledous L, Silva M, Mithieux G, Penicaud L, Lorsignol A, Casteilla L and Dromard C. Pain sensing neurons promote tissue regeneration in adult mice. NPJ Regen Med 2021; 6: 63.
[11] Chernov AV and Shubayev VI. Sexual dimorphism of early transcriptional reprogramming in dorsal root ganglia after peripheral nerve injury. Front Mol Neurosci 2021; 14: 779024.
[12] Mecklenburg J, Zou Y, Wangzhou A, Garcia D, Lai Z, Tumanov AV, Dussor G, Price TJ and Akopian AN. Transcriptomic sex differences in sensory neuronal populations of mice. Sci Rep 2020; 10: 15278.
[13] Tavares-Ferreira D, Shiers S, Ray PR, Wangzhou A, Jeevakumar V, Sankaranarayanan I, Cervantes AM, Reese JC, Chamessian A, Copits BA, Dougherty PM, Gereau RW 4th, Burton MD, Dussor G and Price TJ. Spatial transcriptomics of dorsal root ganglia identifies molecular signatures of human nociceptors. Sci Transl Med 2022; 14: eabj8186.
[14] Arendt-Tranholm A, Mwirigi JM and Price TJ. RNA isoform expression landscape of the human dorsal root ganglion (DRG) generated from long read sequencing. bioRxiv 2023; 2023.10.28.564535.
[15] Ray PR, Shiers S, Caruso JP, Tavares-Ferreira D, Sankaranarayanan I, Uhelski ML, Li Y, North RY, Tatsui C, Dussor G, Burton MD, Dougherty PM and Price TJ. RNA profiling of human dorsal root ganglia reveals sex differences in mechanisms promoting neuropathic pain. Brain 2023; 146: 749-766.
[16] Catala-Senent JF, Andreu Z, Hidalgo MR, Soler-Saez I, Roig FJ, Yanguas-Casas N, Neva-Alejo A, Lopez-Cerdan A, de la Iglesia-Vaya M, Stranger BE and Garcia-Garcia F. A deep transcriptome meta-analysis reveals sex differences in multiple sclerosis. Neurobiol Dis 2023; 181: 106113.
[17] International Multiple Sclerosis Genetics Consortium. Multiple sclerosis genomic map implicates peripheral immune cells and microglia in susceptibility. Science 2019; 365: eaav7188.
[18] Ribbons KA, McElduff P, Boz C, Trojano M, Izquierdo G, Duquette P, Girard M, Grand'Maison F, Hupperts R, Grammond P, Oreja-Guevara C, Petersen T, Bergamaschi R, Giuliani G, Barnett M, van Pesch V, Amato MP, Iuliano G, Fiol M, Slee M, Verheul F, Cristiano E, Fernandez-Bolanos R, Saladino ML, Rio ME, Cabrera-Gomez J, Butzkueven H, van Munster E, Den Braber-Moerland L, La Spitaleri D, Lugaresi A, Shaygannejad V, Gray O, Deri N, Alroughani R and Lechner-Scott J. Male sex is independently associated with faster disability accumulation in relapse-onset ms but not in primary progressive MS. PLoS One 2015; 10: e0122686.
[19] Bove R and Chitnis T. The role of gender and sex hormones in determining the onset and outcome of multiple sclerosis. Mult Scler 2014; 20: 520-526.
[20] Kaplan TB, Gopal A, Block VJ, Suskind AM, Zhao C, Polgar-Turcsanyi M, Saraceno TJ, Gomez R, Santaniello A, Consortium S, Ayoubi NE, Cree BAC, Hauser SL, Weiner H, Chitnis T, Khoury S and Bove R. Challenges to longitudinal characterization of lower urinary tract dysfunction in multiple sclerosis. Mult Scler Relat Disord 2022; 62: 103793.
[21] Case LK, Wall EH, Dragon JA, Saligrama N, Krementsov DN, Moussawi M, Zachary JF, Huber SA, Blankenhorn EP and Teuscher C. The Y chromosome as a regulatory element shaping immune cell transcriptomes and susceptibility to autoimmune disease. Genome Res 2013; 23: 1474-1485.
[22] Maguire AD, Friedman TN, Villarreal Andrade DN, Haq F, Dunn J, Pfeifle K, Tenorio G, Buro K, Plemel JR and Kerr BJ. Sex differences in the inflammatory response of the mouse DRG and its connection to pain in experimental autoimmune encephalomyelitis. Sci Rep 2022; 12: 20995.
[23] Friedman TN, La Caprara O, Zhang C, Lee K, May J, Faig CA, Baldwin T, Plemel JR, Taylor AMW and Kerr BJ. Sex differences in peripheral immune cell activation: Implications for pain and pain resolution. Brain Behav Immun 2023; 114: 80-93.
[24] Friedman TN, Yousuf MS, Catuneanu A, Desai M, Juzwik CA, Fournier AE and Kerr BJ. Profiling the microRNA signature of the peripheral sensory ganglia in experimental autoimmune encephalomyelitis (EAE). J Neuroinflammation 2019; 16: 223.

[25] Correale J, Li S, Weiner LP and Gilmore W. Effect of persistent mouse hepatitis virus infection on MHC class I expression in murine astrocytes. J Neurosci Res 1995; 40: 10-21.
[26] Liu MT, Keirstead HS and Lane TE. Neutralization of the chemokine CXCL10 reduces inflammatory cell invasion and demyelination and improves neurological function in a viral model of multiple sclerosis. J Immunol 2001; 167: 4091-4097.
[27] Bender SJ and Weiss SR. Pathogenesis of murine coronavirus in the central nervous system. J Neuroimmune Pharmacol 2010; 5: 336-354.
[28] Houtman JJ and Fleming JO. Pathogenesis of mouse hepatitis virus-induced demyelination. J Neurovirol 1996; 2: 361-376.
[29] Dandekar AA, Anghelina D and Perlman S. Bystander CD8 T-cell-mediated demyelination is interferon-gamma-dependent in a coronavirus model of multiple sclerosis. Am J Pathol 2004; 164: 363-369.
[30] Dandekar AA, Wu GF, Pewe L and Perlman S. Axonal damage is T cell mediated and occurs concomitantly with demyelination in mice infected with a neurotropic coronavirus. J Virol 2001; 75: 6115-6120.
[31] McMillan MT, Pan XQ, Smith AL, Newman DK, Weiss SR, Ruggieri MR Sr and Malykhina AP. Coronavirus-induced demyelination of neural pathways triggers neurogenic bladder overactivity in a mouse model of multiple sclerosis. Am J Physiol Renal Physiol 2014; 307: F612-622.
[32] Lamarre NS, Braverman AS, Malykhina AP, Barbe MF and Ruggieri MR Sr. Alterations in nerve-evoked bladder contractions in a coronavirus-induced mouse model of multiple sclerosis. PLoS One 2014; 9: e109314.
[33] Lee S, Nedumaran B, Hypolite J, Caldwell B, Rudolph MC and Malykhina AP. Differential neurodegenerative phenotypes are associated with heterogeneous voiding dysfunction in a coronavirus-induced model of multiple sclerosis. Sci Rep 2019; 9: 10869.
[34] Manaker RA, Piczak CV, Miller AA and Stanton MF. A hepatitis virus complicating studies with mouse leukemia. J Natl Cancer Inst 1961; 27: 29-51.
[35] Cima G. AVMA guidelines for the euthanasia of animal: 2013 edition. Javma-Journal of the American Veterinary Medical Association 2013; 242: 715-716.
[36] Baskozos G, Dawes JM, Austin JS, Antunes-Martins A, McDermott L, Clark AJ, Trendafilova T, Lees JG, McMahon SB, Mogil JS, Orengo C and Bennett DL. Comprehensive analysis of long noncoding RNA expression in dorsal root ganglion reveals cell-type specificity and dysregulation after nerve injury. Pain 2019; 160: 463-485.
[37] Bailey AL and Ribeiro-da-Silva A. Transient loss of terminals from non-peptidergic nociceptive fibers in the substantia gelatinosa of spinal cord following chronic constriction injury of the sciatic nerve. Neuroscience 2006; 138: 675-690.
[38] Sorge RE, Mapplebeck JC, Rosen S, Beggs S, Taves S, Alexander JK, Martin LJ, Austin JS, Sotocinal SG, Chen D, Yang M, Shi XQ, Huang H, Pillon NJ, Bilan PJ, Tu Y, Klip A, Ji RR, Zhang J, Salter MW and Mogil JS. Different immune cells mediate mechanical pain hypersensitivity in male and female mice. Nat Neurosci 2015; 18: 1081-1083.
[39] Gal-Oz ST, Maier B, Yoshida H, Seddu K, Elbaz N, Czysz C, Zuk O, Stranger BE, Ner-Gaon H and Shay T. ImmGen report: sexual dimorphism in the immune system transcriptome. Nat Commun 2019; 10: 4295.
[40] Sorge RE, LaCroix-Fralish ML, Tuttle AH, Sotocinal SG, Austin JS, Ritchie J, Chanda ML, Graham AC, Topham L, Beggs S, Salter MW and Mogil JS. Spinal cord Toll-like receptor 4 mediates inflammatory and neuropathic hypersensitivity in male but not female mice. J Neurosci 2011; 31: 15450-15454.
[41] Bell MR. Comparing postnatal development of gonadal hormones and associated social behaviors in rats, mice, and humans. Endocrinology 2018; 159: 2596-2613.
[42] Mauvais-Jarvis F, Arnold AP and Reue K. A guide for the design of pre-clinical studies on sex differences in metabolism. Cell Metab 2017; 25: 1216-1230.
[43] De Vries GJ, Rissman EF, Simerly RB, Yang LY, Scordalakes EM, Auger CJ, Swain A, Lovell-Badge R, Burgoyne PS and Arnold AP. A model system for study of sex chromosome effects on sexually dimorphic neural and behavioral traits. J Neurosci 2002; 22: 9005-9014.
[44] Link JC, Chen X, Arnold AP and Reue K. Metabolic impact of sex chromosomes. Adipocyte 2013; 2: 74-79.
[45] Moon S, Alsarkhi L, Lin TT, Inoue R, Tahiri A, Colson C, Cai W, Shirakawa J, Qian WJ, Zhao JY and El Ouaamari A. Transcriptome and secretome profiling of sensory neurons reveals sex differences in pathways relevant to insulin sensing and insulin secretion. FASEB J 2023; 37: e23185.
[46] Barry AM, Zhao N, Yang X, Bennett DL and Baskozos G. Deep RNA-seq of male and female murine sensory neuron subtypes after nerve injury. Pain 2023; 164: 2196-2215.
[47] Clanet M, Blancher A, Calvas P and Rascol O. Interferons and multiple sclerosis. Biomed Pharmacother 1989; 43: 355-360.
[48] Reder AT and Feng X. How type I interferons work in multiple sclerosis and other diseases:

some unexpected mechanisms. J Interferon Cytokine Res 2014; 34: 589-599.
[49] Finkelsztejn A. Multiple sclerosis: overview of disease-modifying agents. Perspect Medicin Chem 2014; 6: 65-72.
[50] Zaroon, Aslam S, Hafsa, Mustafa U, Fatima S and Bashir H. Interleukin in immune-mediated diseases: an updated review. Mol Biotechnol 2024.
[51] Suvieri C and Volpi C. Analysis of differential TLR activation in a mouse model of multiple sclerosis. Methods Mol Biol 2023; 2700: 229-247.
[52] Lund JM, Alexopoulou L, Sato A, Karow M, Adams NC, Gale NW, Iwasaki A and Flavell RA. Recognition of single-stranded RNA viruses by Toll-like receptor 7. Proc Natl Acad Sci U S A 2004; 101: 5598-5603.
[53] Hundeshagen A, Hecker M, Paap BK, Angerstein C, Kandulski O, Fatum C, Hartmann C, Koczan D, Thiesen HJ and Zettl UK. Elevated type I interferon-like activity in a subset of multiple sclerosis patients: molecular basis and clinical relevance. J Neuroinflammation 2012; 9: 140.
[54] Dubik M, Marczynska-Grzelak J, Sorensen MZ, Dieu RS, Rusin D, Schioth ES, Ramazani B, Belal R, Ojha B, Krieger J, Arengoth DS, Wlodarczyk A, Owens T and Khorooshi R. Synergistic targeting of innate receptors tlr7 and nod2 for therapeutic intervention in multiple sclerosis. Int J Mol Sci 2024; 25: 7462.
[55] Banisor I, Leist TP and Kalman B. Involvement of beta-chemokines in the development of inflammatory demyelination. J Neuroinflammation 2005; 2: 7.
[56] Dhaiban S, Al-Ani M, Elemam NM and Maghazachi AA. Targeting chemokines and chemokine receptors in multiple sclerosis and experimental autoimmune encephalomyelitis. J Inflamm Res 2020; 13: 619-633.
[57] Mahad DJ, Howell SJ and Woodroofe MN. Expression of chemokines in the CSF and correlation with clinical disease activity in patients with multiple sclerosis. J Neurol Neurosurg Psychiatry 2002; 72: 498-502.
[58] Schall TJ, Bacon K, Toy KJ and Goeddel DV. Selective attraction of monocytes and T lymphocytes of the memory phenotype by cytokine RANTES. Nature 1990; 347: 669-671.
[59] Clarkson TC, Iguchi N, Xie AX and Malykhina AP. Differential transcriptomic changes in the central nervous system and urinary bladders of mice infected with a coronavirus. PLoS One 2022; 17: e0278918.
[60] Furuta A, Yamamoto T, Suzuki Y, Gotoh M, Egawa S and Yoshimura N. Comparison of inflammatory urine markers in patients with interstitial cystitis and overactive bladder. Int Urogynecol J 2018; 29: 961-966.
[61] Gonzalez EJ, Arms L and Vizzard MA. The role(s) of cytokines/chemokines in urinary bladder inflammation and dysfunction. Biomed Res Int 2014; 2014: 120525.
[62] Lopes Fischer N, Naseer N, Shin S and Brodsky IE. Effector-triggered immunity and pathogen sensing in metazoans. Nat Microbiol 2020; 5: 14-26.
[63] Tretina K, Park ES, Maminska A and MacMicking JD. Interferon-induced guanylate-binding proteins: guardians of host defense in health and disease. J Exp Med 2019; 216: 482-500.
[64] Ye F, Liang J, Li J, Li H and Sheng W. Development and validation of a five-gene signature to predict relapse-free survival in multiple sclerosis. Front Neurol 2020; 11: 579683.
[65] Guo H, Li Z and Wang Y. BCL3, GBP1, IFI16, and CCR1 as potential brain-derived biomarkers for parietal grey matter lesions in multiple sclerosis. Sci Rep 2024; 14: 28543.
[66] Rahmat-Zaie R, Amini J, Haddadi M, Beyer C, Sanadgol N and Zendedel A. TNF-alpha/STAT1/CXCL10 mutual inflammatory axis that contributes to the pathogenesis of experimental models of multiple sclerosis: a promising signaling pathway for targeted therapies. Cytokine 2023; 168: 156235.
[67] Freedman MS, Ruijs TC, Blain M and Antel JP. Phenotypic and functional characteristics of activated CD8+ cells: a CD11b-CD28- subset mediates noncytolytic functional suppression. Clin Immunol Immunopathol 1991; 60: 254-267.
[68] Alarcon B, Gil D, Delgado P and Schamel WW. Initiation of TCR signaling: regulation within CD3 dimers. Immunol Rev 2003; 191: 38-46.
[69] Zuo M, Fettig NM, Bernier LP, Possnecker E, Spring S, Pu A, Ma XI, Lee DS, Ward LA, Sharma A, Kuhle J, Sled JG, Probstel AK, MacVicar BA, Osborne LC, Gommerman JL and Ramaglia V. Age-dependent gray matter demyelination is associated with leptomeningeal neutrophil accumulation. JCI Insight 2022; 7: e158144.
[70] Serhan N, Cenac N, Basso L and Gaudenzio N. Mas-related G protein-coupled receptors (Mrgprs) - Key regulators of neuroimmune interactions. Neurosci Lett 2021; 749: 135724.
[71] Porebski G, Kwiecien K, Pawica M and Kwitniewski M. Mas-related G protein-coupled receptor-X2 (MRGPRX2) in drug hypersensitivity reactions. Front Immunol 2018; 9: 3027.
[72] Tronik-Le Roux D, Senorale-Pose M and Rougeon F. Three novel SMR1-related cDNAs characterized in the submaxillary gland of mice show extensive evolutionary divergence in the protein coding region. Gene 1994; 142: 175-182.
[73] Qi L, Iskols M, Shi D, Reddy P, Walker C, Lezgiyeva K, Voisin T, Pawlak M, Kuchroo VK, Chiu IM, Ginty DD and Sharma N. A mouse

DRG genetic toolkit reveals morphological and physiological diversity of somatosensory neuron subtypes. Cell 2024; 187: 1508-1526, e16.
[74] Loos RJ. The genetics of adiposity. Curr Opin Genet Dev 2018; 50: 86-95.
[75] Li C, Sun XN, Funcke JB, Vanharanta L, Joffin N, Li Y, Prasanna X, Paredes M, Joung C, Gordillo R, Voros C, Kulig W, Straub L, Chen S, Velasco J, Cobb A, Padula D, Wang MY, Onodera T, Varlamov O, Li Y, Liu C, Nawrocki AR, Zhao S, Oh DY, Wang ZV, Goodman JM, Wynn RM, Vattulainen I, Han Y, Ikonen E and Scherer PE. Adipogenin dictates adipose tissue expansion by facilitating the assembly of a dodecameric seipin complex. bioRxiv 2024; 2024.07.25.605195.
[76] Peruzzotti-Jametti L, Bernstock JD, Vicario N, Costa ASH, Kwok CK, Leonardi T, Booty LM, Bicci I, Balzarotti B, Volpe G, Mallucci G, Manferrari G, Donega M, Iraci N, Braga A, Hallenbeck JM, Murphy MP, Edenhofer F, Frezza C and Pluchino S. Macrophage-derived extracellular succinate licenses neural stem cells to suppress chronic neuroinflammation. Cell Stem Cell 2018; 22: 355-368, e13.
[77] Ni W, Ramalingam M, Li Y, Park JH, Dashnyam K, Lee JH, Bloise N, Fassina L, Visai L, De Angelis MGC, Pedraz JL, Kim HW and Hu J. Immunomodulatory and anti-inflammatory effect of neural stem/progenitor cells in the central nervous system. Stem Cell Rev Rep 2023; 19: 866-885.
[78] Villalon Landeros E, Kho SC, Church TR, Brennan A, Turker F, Delannoy M, Caterina MJ and Margolis SS. The nociceptive activity of peripheral sensory neurons is modulated by the neuronal membrane proteasome. Cell Rep 2024; 43: 114058.
[79] Paubel A, Marouillat S, Dangoumau A, Maurel C, Haouari S, Blasco H, Corcia P, Laumonnier F, Andres CR and Vourc'h P. Dynamic expression of genes Encoding Ubiquitin Conjugating Enzymes (E2s) during neuronal differentiation and maturation: implications for neurodevelopmental disorders and neurodegenerative diseases. Genes (Basel) 2024; 15: 1381.
[80] Xu F, Gao W, Zhang M, Zhang F, Sun X, Wu B, Liu Y, Li X and Li H. Diagnostic implications of ubiquitination-related gene signatures in Alzheimer's disease. Sci Rep 2024; 14: 10728.
[81] Krementsov DN, Katchy A, Case LK, Carr FE, Davis B, Williams C and Teuscher C. Studies in experimental autoimmune encephalomyelitis do not support developmental bisphenol a exposure as an environmental factor in increasing multiple sclerosis risk. Toxicol Sci 2013; 135: 91-102.
[82] Wei T, Wang Y, Xu W, Liu Y, Chen H and Yu Z. KCa3.1 deficiency attenuates neuroinflammation by regulating an astrocyte phenotype switch involving the PI3K/AKT/GSK3beta pathway. Neurobiol Dis 2019; 132: 104588.
[83] Hovhannisyan AH, Son H, Mecklenburg J, Barba-Escobedo PA, Tram M, Gomez R, Shannonhouse J, Zou Y, Weldon K, Ruparel S, Lai Z, Tumanov AV, Kim YS and Akopian AN. Pituitary hormones are specifically expressed in trigeminal sensory neurons and contribute to pain responses in the trigeminal system. Sci Rep 2021; 11: 17813.